Experimental Study of Fiber-Reinforced Sand Subject to Seepage

K.-H. Yang[1]([✉]), W.M. Adilehou[2], S.-T. Jian[2], and B.-C. Hsiung[3]

[1] Department of Civil Engineering, National Taiwan University, Taipei, Taiwan
khyang@ntu.edu.tw
[2] Department of Civil and Construction Engineering,
National Taiwan University of Science and Technology, Taipei, Taiwan
[3] Department of Civil Engineering,
National Kaohsiung University of Applied Science, Kaohsoung, Taiwan

Abstract. This paper presents an experimental study on the hydraulic responses of fiber-reinforced soil (FRS) subject to seepage. A series of upward seepage tests on unreinforced and reinforced sand was conducted to investigate the influence of soil density and fiber parameters (i.e., fiber contents and lengths) on the piping failure mode, hydraulic conductivity k, and critical hydraulic gradient i_{cr} of FRS. Direct shear tests were also performed to establish the relationships between soil shear strength and critical hydraulic gradient of FRS. The seepage test results revealed that k decreases and i_{cr} increases as the fiber content increases. Short fiber appears to reduce k; however, the fiber length has only a minor influence on the i_{cr}. The fiber has a greater effect on dense specimens than it does on loose specimens. The test results also indicate the i_{cr} of FRS is strongly correlated to its soil shear strength. The findings in this study suggest that the use of FRS as backfill in hydraulic structures can effectively delay the advance of seepage, reduce soil piping potential, and improve system stability against seepage. The results and discussion in this study provide insightful information for the application of FRS to hydraulic structures.

Keywords: Fiber-reinforced sand · Critical hydraulic gradient · Hydraulic conductivity · Soil shear strength

1 Introduction

Hydraulic failures of geotechnical earth structures are caused by impacts from wave forces, toe scour, overtopping, and soil piping and erosion (Brandl 2011). As taller hydraulic structures are constructed because of rising flood levels due to the influence of global warming and extreme weather, the increasing hazards of soil piping and erosion have gained much attention (Danka and Zhang 2015).

Past case studies have reported that failures of many manmade earth fill structures, natural soil masses, and rock deposits (e.g., landslide dams) have been associated with seepage-induced piping and erosion (Foster et al. 2000). Consequently, mitigating seepage-induced adverse impacts and enhancing the stability of the earth structures has become an urgent and challenging issue in waterfront protection.

Effective countermeasures against soil piping involve the use of cut-off walls, impervious blankets, and pressure relief wells to reduce the hydraulic gradient within the soil or the use of soil improvement and filter layers to increase soil piping resistance. Among these measures, soil improvement through fiber reinforcement is the focus of this study.

The majority of previous studies have focused on the mechanical behavior of fiber-reinforced soil (FRS) and demonstrated that mixing fiber with soil can effectively enhance peak shear strength and reduce the loss of postpeak shear strength (Consoli et al. 2009; Michalowski and Čermák 2003; Zornberg 2002). Soil type, fiber type, length, and content, as well as cement content and compaction conditions, are the key parameters evaluated in these studies (Chou et al. 2016).

In contrast to the studies on mechanical behavior of FRS, studies on the hydraulic performance of FRS are relatively limited. Only a few studies of experimental seepage tests on FRS (Das et al. 2009; Das and Viswanadham 2010; Estabragh et al. 2014, 2016; Furumoto et al. 2002; Sivakumar Babu and Vasudevan 2008) and model tests for levees reinforced with short fibres (Furumoto et al. 2002) have been reported in the literature. In summary, these studies have found that fiber reinforcement can effectively enhance the piping resistance of soil by deferring the occurrence of soil piping at a high hydraulic gradient. Little attention has focused on the effect of fiber parameters on the hydraulic conductivity of FRS, which is another crucial hydraulic parameter of FSR. The preceding discussion is the basis of this study, which involved conducting a series of upward seepage tests on unreinforced and reinforced sands. The objectives of this study are as follows: (1) to evaluate the influence of soil density and fiber parameters (i.e., fiber length and content) on the hydraulic responses (i.e., piping failure mode, hydraulic conductivity, and critical hydraulic gradient) of FRS; and (2) to establish the relationship between the critical hydraulic gradient and the shear strength parameter of FRS. The results and discussion in this study provide insightful information for the application of FRS to hydraulic structures.

2 Experimental Program

2.1 Test System

A series of seepage tests were conducted to evaluate the influences of soil density and fiber parameters on the hydraulic conductivity and critical hydraulic gradient of FRS. For this purpose, an upward seepage test system (Fig. 1), consisting of a constant head device, a permeameter, and measuring systems, was developed in this study and is described in this section.

The permeameter consists of a cylindrical cell (10.5 cm in diameter and 38 cm in height) and a bottom pedestal. To avoid a scale effect, the ratios of the specimen diameter to the mean grain diameter of sand in this test were 90, which is larger than the values (8–12) specified in ASTM (D2434). Additionally, the diameter of the specimen (i.e., 10.5 cm) also satisfies the ASTM requirement (i.e., cylinder diameter >7.6 cm) with respect to the grain sizes of the used soils. The pedestal, filled with marbles and covered with porous screens was used to distribute the upward seepage
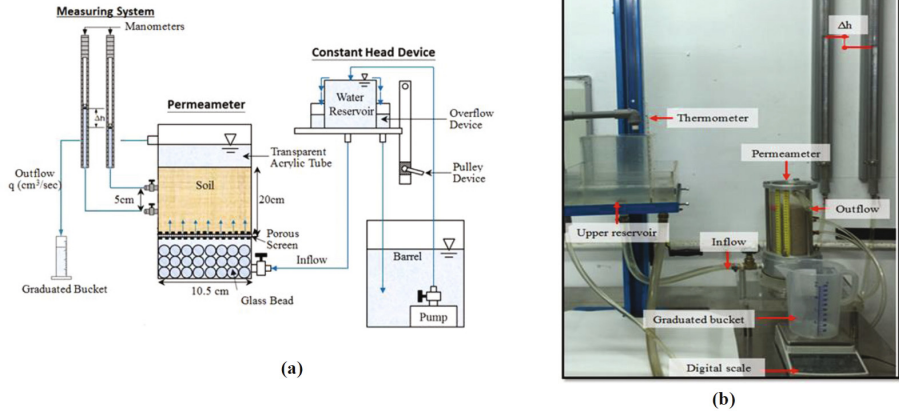
Fig. 1. Upward seepage test system: (a) schematic illustration; (b) overview photo

evenly across the soil specimen. The porous screens comprised two perforated metal plates and a nonwoven geotextile. The perforated metal plates, with numerous punched holes, were used to support the overburden pressure from soil specimens. The non-woven geotextile was placed between the two perforated metal plates and served as a filter to prevent the loss of soil.

The water flow from the top of the specimen was measured and then discharged to the barrel. Discharge velocity v at a given hydraulic gradient was calculated by dividing the collected volume of discharge at a certain time period by the cross-sectional area of the soil specimen. The permeameter cylinder was perforated at distances of 7 and 12 cm from the bottom of the specimen (Fig. 1) and connected to graduated manometers to measure hydraulic head difference (i.e., head loss) at a given distance of the seepage path. The corresponding hydraulic gradient i can then be calculated at each stage of the test using the following equation:

$$i = \frac{\Delta h}{L} \tag{1}$$

where Δh is the head difference between two manometers and L (=5 cm) is the distance between the two measuring valves connected to the manometers.

2.2 Test Material and Test Program

Uniform quartz sand was tested in this study. Figure 2 presents the grain size distribution curve of the test soil. Table 1 summarizes the soil properties. The minimum and maximum dry unit weights of sand, conducted in accordance with ASTM (D4254, D4253) at the two target relative densities (D_r = 50% and 70%) to represent soil loose and dense conditions, were $\gamma_{d,min}$ = 13.92 kN/m^3 and $\gamma_{d,max}$ = 15.35 kN/m^3. Based on
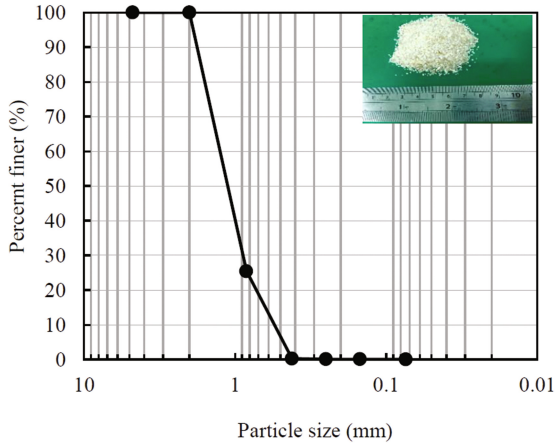
Fig. 2. Grain size distribution curve and photo of the tested sand

Table 1. Summary of test soil properties

Soil properties	Value
Specific gravity G_s	2.65
Effective particle size d_{10} (mm)	0.61
Mean particle size d_{50} (mm)	1.12
Uniformity coefficient C_u	2.02
Coefficient of curvature C_c	1.08
Soil classification (USCS)	SP
Maximum dry unit weight $\gamma_{d,max}$ (kN/m³)	15.35
Minimum dry unit weight $\gamma_{d,min}$ (kN/m³)	13.92
Maximum void ratio e_{max}	0.87
Minimum void ratio e_{min}	0.63
[a]Hydraulic conductivity of soil k (m/s)	8.2×10^{-3} and 6.1×10^{-3}
[a]Critical hydraulic gradient of soil i_{cr}	0.86 and 0.92

[a] Values are for soil density D_r = 50% and 70%, respectively.

the constant head test results presented later, the saturated hydraulic conductivity of the soil was $k = 8.2 \times 10^{-3}$ and 6.1×10^{-3} m/s, and the critical hydraulic gradient of the soil was i_{cr} = 0.86 and 0.92 for soil at D_r = 50% and 70%, respectively.

Polypropylene (PP) fiber was used in this study. PP fiber is the most widely adopted synthetic fiber for soil reinforcement (Yetimoglu et al. 2003; Hejazi et al. 2012). Das and Viswanadham (2010) reported that PP fiber performed better than polyester (PET) fiber in increasing seepage resistance. It is because the PET fiber has a specific gravity higher than the PP fiber. For the same fiber content, a larger specific gravity implies a lower fiber volume and a less number of fibers, and hence reduces the benefit

of improving the piping resistance of a soil. The PP fiber tested in this study has a circular cross-section with an average diameter of 0.0577 mm. The specific gravity of the fiber is $G_{sf} = 0.91$, slightly lower than that of water. Table 2 summarizes the physical and mechanical properties of the test fiber. A total of 20 seepage tests were conducted on both unreinforced and reinforced soil specimens. The test variables are

Table 2. Physical and mechanical properties of fiber

Properties	Value
Type	Polypropylene (PP) fiber
Cross-section shape	Circular
Equivalent diameter d_f (mm)	0.0557
Length L_f (mm)	6, 12, 19
Specific gravity G_{sf}	0.91
Denier (g/9000 m)	20
Ultimate tensile strength (MPa)	250
Melting point (°C)	160–170
Water absorption	No

Table 3. Summary of seepage test conditions and results

Test	ω_f (%)	L_f (mm)	i_{cr}	i_{cr} ratio	k (m/s)	k ratio
Test Series L (Loose Specimen)						
U-50	0	0	0.86	1	8.2×10^{-3}	1
R-50-0.5-6	0.5	6	1.16	1.35	4.3×10^{-3}	0.52
R-50-1-6	1	6	1.2	1.40	3.7×10^{-3}	0.45
R-50-1.5-6	1.5	6	1.52	1.77	2.2×10^{-3}	0.27
R-50-0.5-12	0.5	12	1.08	1.26	5.3×10^{-3}	0.65
R-50-1-12	1	12	1.3	1.51	4.4×10^{-3}	0.54
R-50-1.5-12	1.5	12	1.52	1.77	3.2×10^{-3}	0.39
R-50-0.5-19	0.5	19	1.14	1.33	6.5×10^{-3}	0.79
R-50-1-19	1	19	1.34	1.56	3.9×10^{-3}	0.48
R-50-1.5-19	1.5	19	1.36	1.58	3.5×10^{-3}	0.43
Test Series D (Dense Specimen)						
U-70	0	0	0.92	1	6.1×10^{-3}	1
R-70-0.5-6	0.5	6	1.28	1.39	4.1×10^{-3}	0.68
R-70-1-6	1	6	1.40	1.52	2.8×10^{-3}	0.46
R-70-1.5-6	1.5	6	1.94	2.11	1.4×10^{-3}	0.24
R-70-0.5-12	0.5	12	1.22	1.33	3.3×10^{-3}	0.54
R-70-1-12	1	12	1.50	1.63	3.1×10^{-3}	0.51
R-70-1.5-12	1.5	12	1.74	1.89	2.5×10^{-3}	0.41
R-70-0.5-19	0.5	19	1.28	1.39	4.1×10^{-3}	0.67
R-70-1-19	1	19	1.36	1.48	3.3×10^{-3}	0.54
R-70-1.5-19	1.5	19	1.62	1.76	2.5×10^{-3}	0.41

soil relative density ($D_r = 50\%$ and 70%), fiber content ($\omega_f = 0\%$, 0.5%, 1.0%, and 1.5%), and fiber length ($L_f = 6$, 12, and 19 mm).

Table 3 lists the seepage test program. The test numbering was defined as follows. The first part, a letter "R" or "U," indicates a reinforced or unreinforced specimen, respectively. The second, third, and fourth parts denote soil relative density, fiber content, and fiber length, respectively. For example, U-50 indicates an unreinforced specimen with soil relative density $D_r = 50\%$ and R-70-0.5-6 indicates a reinforced specimen with soil relative density $D_r = 70\%$, fiber content $\omega_f = 0.5\%$ and fiber length $L_f = 6$ mm.

2.3 Specimen Preparation and Test Procedure

The specimens were prepared at loose and dense conditions (i.e., Test Series L and D), corresponding to soil relative density $D_r = 50\%$ and 70%. Each specimen was carefully prepared to ensure that its soil had a uniform density and full saturation. The required weight of dry soil for the target relative density was determined using the relative density equation:

$$D_r = \frac{e_{\max} - e}{e_{\max} - e_{\min}} \qquad (2)$$

where e_{max}, e_{min}, and e are the maximum, minimum, and target void ratios of soil. The desired weight of fiber for reinforced specimens was determined considering the dry weight of the soil and the desired gravimetric fiber content, as expressed in Eq. (3):

$$\omega_f = \frac{W_f}{W_s} \qquad (3)$$

where W_f and W_s are the dry weight of fiber and soil, respectively.

A known quantity of soil and fiber was carefully mixed by hand. The hand mixing method has been commonly adopted by various researchers (Yetimoglu and Salbas 2003; Das et al. 2009; Estabragh et al. 2014). The soil–fiber mixture was moisturized by adding water (10% of total weight) to avoid soil–fiber segregation before being spread into the permeameter. The permeameter was carefully filled with the wet soil–fiber mixture in five layers (4-cm thick for each layer). Each layer was slightly compacted using a metal rod to control its height. This procedure was repeated until the desired specimen height ($H = 20$ cm) was reached. Visual inspection showed that good uniformity was achieved. The repeatability and consistency of the test results were verified by examining test results performed under the same conditions.

Figure 3 shows the scanning electron microscope (SEM) photographs of unreinforced specimens at different relative densities (Figs. 3a and b) and the FRS specimen of R-70-1-6 (Fig. 3c). The interaction between fibers and soil grains can be clearly observed from Fig. 3c. Compared with unreinforced sand, some soil pore spaces (as highlighted by red dashed lines in Fig. 3c) of the reinforced sand were partially filled by the fibers. Consequently, the fibers could block some pore channels for seepage and restrict the seepage flow within these pore channels.
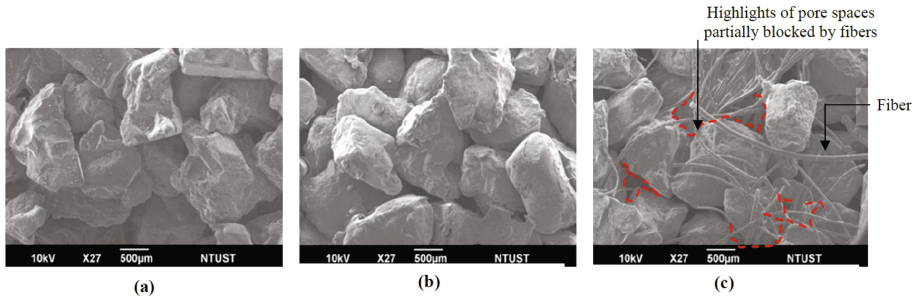
Fig. 3. Scanning electron microscope (SEM) photo: (a) unreinforced sand at $D_r = 50\%$ (U-50); (b) unreinforced sand at $D_r = 70\%$ (U-70); (c) fiber-reinforced sand (R-70-1-6)

After specimen preparation, the specimen was submerged in water and subjected to a constant seepage flow under a low hydraulic head that did not affect the specimen stability for 24 h to ensure the full saturation of specimens. Afterward, the seepage test began by applying a series of incrementally increased hydraulic heads to the specimen until soil piping failure occurred. The applied hydraulic head was increased by 2 cm (approximately $\Delta i = 0.1$) for each increment and maintained for at least 10 min until the hydraulic heads in the manometers stabilized, indicating that equilibrium was reached. The hydraulic gradient i and corresponding discharge velocity v were recorded in each stage of the test.

3   Results and Discussion

In this section, the test results including seepage failure mode and the i–v relations were analyzed and discussed. The i–v plots were used to determine the k and i_{cr} of FRS. The influence of soil density and fiber parameters on the hydraulic responses of FRS is quantitatively evaluated and discussed, and the relationship between the critical hydraulic gradient and the shear strength of FRS is established.

3.1   Failure Modes

Figure 4 shows the typical failure modes of unreinforced and reinforced specimens at and after the critical hydraulic gradient i_{cr}. For the unreinforced specimen at i_{cr} (Fig. 4a), the specimen (U-70) exhibited an expansion (≈ 0.8 cm). At this stage, the soil seemed to have liquefied (the author's finger can easily penetrate into the specimen without feeling much resistance). When the next hydraulic head increment after i_{cr} was applied, the specimen showed a sudden and notable heave (≈ 2 cm), following by the sand piping/boiling phenomenon (Fig. 4b). The soil lost it overall stability. The heave and boiling phenomenon are strong evidence of soil failure subjected to seepage. The soil boiling happened globally within the unreinforced specimen in which soil particles were forced to migrate with the upward seepage. Vigorous soil boiling on top of the specimen can also be clearly observed.
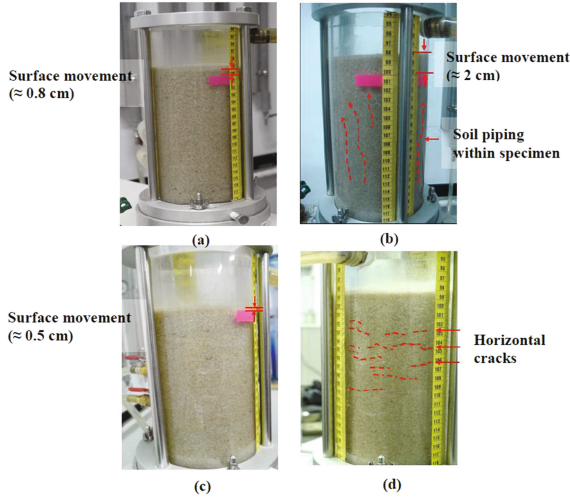
Fig. 4. Failure mode of unreinforced and reinforced specimens: (a) U-70 at i_{cr} = 0.92; (b) U-70 at the next applied hydraulic head increment after i_{cr}; (c) R-70-1.5-19 at i_{cr} = 1.62; (d) development of horizontal cracks of R-70-1.5-19 at the next applied hydraulic head increment after i_{cr}

For the reinforced specimen at i_{cr} (Fig. 4c), the specimen (R-70-1.5-19) displayed an isotropic failure mode: soil experienced a uniformly slight heave (≈0.5 cm). At this stage (onset of soil seepage failure), the surface movement of the reinforced specimen is smaller than that of the unreinforced specimen even though the reinforced specimen was subject to a seepage force (i_{cr} = 1.62) higher than that of the unreinforced specimen (i_{cr} = 0.92). Figure 4d shows the failure mode of the reinforced specimen when the next hydraulic head increment after i_{cr} was applied. Several horizontal micro cracks developed within the specimen at this stage.

The development of horizontal cracks within the reinforced specimen indicates significant distress on the specimen upon seepage force. The observed horizontal cracks also reveal that the seepage force induced tensile force could have exceeded the tensile resistance provided by fibers at local areas within the specimen; consequently, soil particles at these areas tend to separate and then the cracks develop. Unlike the failure mode of the unreinforced specimen, the reinforced specimen experienced neither global soil piping within the specimen nor vigorous soil boiling on top of the specimen. This observation demonstrates that fiber can effectively bind soil together against seepage and convert the vigorous soil erosion and piping in the unreinforced soil to a global and isotropic soil expansion.

3.2 I–V Relations

Figures 5 and 6 show the i–v plots for different soil densities, fiber contents, and fiber lengths. The i–v curves consist of two parts. At the first part of the curves, the v value increases linearly with i. The flow is laminar and the hydraulic conductivity k can be

obtained according to Darcy's law (i.e., $v = ki$). At the second part of the curves, the i–v curves exhibit either a drastic increase in the discharge velocity or a decrease in the measured hydraulic gradient. Both phenomena indicate a change in the hydraulic behavior of specimens, suggesting the occurrence of the soil seepage failure. The critical hydraulic gradient was determined at one stage prior to this stage. Table 3 summarizes the test results of k and i_{cr}.

Although the system total head was increased by elevating the upper water reservoir, the drop in the hydraulic gradient after i_{cr} suggests the relief of accumulated pore water pressure within specimens after soil piping failure (Fig. 4a) and the development of horizontal cracks (Fig. 4d). The drop can also be explained by the fact that the head
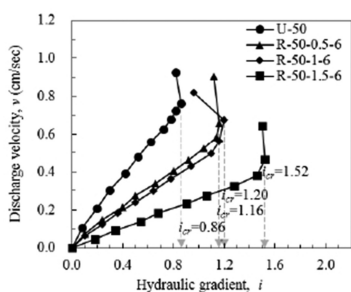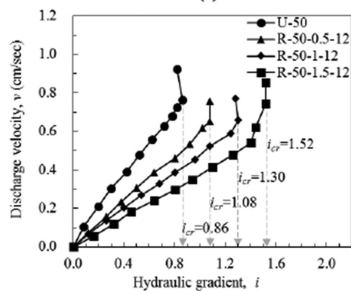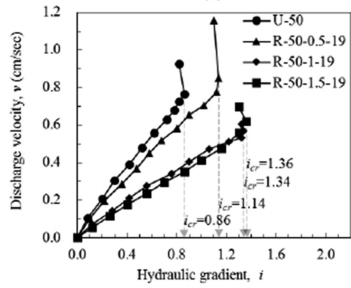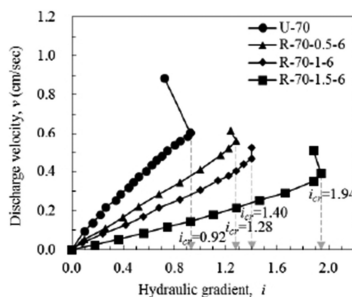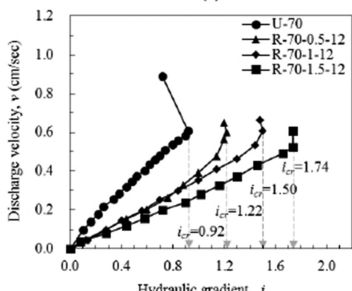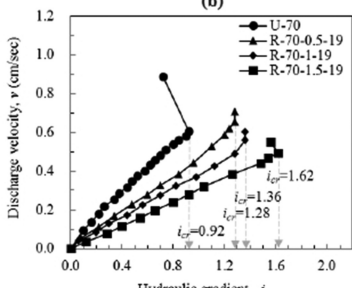
Fig. 5. Results for Test Series L:(a) $L_f = 6$ mm; (b) $L_f = 12$ mm; (c) $L_f = 19$ mm

Fig. 6. Results for Test Series D:(a) $L_f = 6$ mm; (b) $L_f = 12$ mm; (c) $L_f = 19$ mm

loss of seepage through specimens decreased because of the loosened soil packing state after the soil seepage failure. A pressure drop has also been observed in experimental and field tests (Parekh et al. 2016). Consequently, the water pressure measured at this stage cannot represent the real hydraulic conditions.

Figures 5 and 6 clearly reveal that for specimens at the same relative density and fiber length, the i–v curves shift to the right as the fiber content increases, signifying an increase in i_{cr} and a decrease in k. The experimental results likely result from the fiber inclusion providing tensile resistance against soil piping and erosion, and restricting the seepage flow within some pore channels which were partially blocked by fibers. An increase in the critical hydraulic gradient of FRS with fiber content was also reported in Das et al. (2009), Das and Viswanadham (2010), Estabragh et al. (2014, 2016), and Sivakumar Babu and Vasudevan (2008). A detailed and quantitative evaluation of the effect of fiber content and length follows in the next section.

3.3   Effect of Fiber Parameters

This section discusses the effect of fiber parameters (i.e., fiber content and length) on the hydraulic response of FRS. The variation of k and i_{cr} with fiber parameters was quantitatively evaluated using the k and i_{cr} ratios, defined as the ratios of the hydraulic conductivity and critical hydraulic gradient of FRS to those of unreinforced sand. The k and i_{cr} ratios serve as indices for assessing the reduction of seepage velocity and improvement of soil piping resistance.

Figure 7 shows the influence of fiber content on k and i_{cr} and Table 3 lists the associated k and i_{cr} ratio values. A clear trend of increasing i_{cr} and decreasing k with increasing fiber content can be observed, regardless of soil density. For example, for FRS with $L_f = 6$ mm in Test Series L, the k decreases from 8.2×10^{-3} to 2.2×10^{-3} m/s (k ratio decreases from 1.0 to 0.27) and the i_{cr} increases from 0.86 to 1.52 (i_{cr} ratio increases from 1.0 to 1.77) as the fiber content increases from 0 to 1.5%. These results suggest that soil piping resistance increases to 177% of, and hydraulic conductivity decreases to 27% of that of unreinforced sand after adding 1.5% of fiber to the soil. Similarly, for FRS with $L_f = 6$ mm in Test Series D, the k decreases from 6.1×10^{-3} to 1.4×10^{-3} m/s (k ratio decreases from 1.0 to 0.24) and the i_{cr} increases from 0.92 to 1.94 (i_{cr} ratio increases from 1.0 to 2.11) as the fiber content increases from 0 to 1.5%.

The test results also reveal that the fiber has a greater effect in dense specimens (Test Series D) than in loose specimens (Test Series L); at a given fiber length and content, the larger i_{cr} and smaller k values were measured for dense specimens. The high i_{cr} improvement likely results from increased soil–fiber interaction in dense soil states, and high k reduction is attributable to the fact that the pore space of soil in a dense state, which is less abundant and smaller than that of soil in a loose state, could be easily blocked or filled with a given amount of fiber.

Figure 8 shows the influence of fiber length on k and i_{cr} and Table 3 lists the associated k and i_{cr} ratio values. In general, the k values appear to decrease with a decrease in fiber length for specimens at both densities (Fig. 8a and b). That is, compared with long fiber, the short fiber can produce higher k reduction. For example, for FRS with $\omega_f = 1.5\%$, the k increases from 2.2×10^{-3} to 3.5×10^{-3} m/s (k ratio increases from 0.27 to 0.43) in Test Series L and from 1.4×10^{-3} to 2.5×10^{-3} m/s
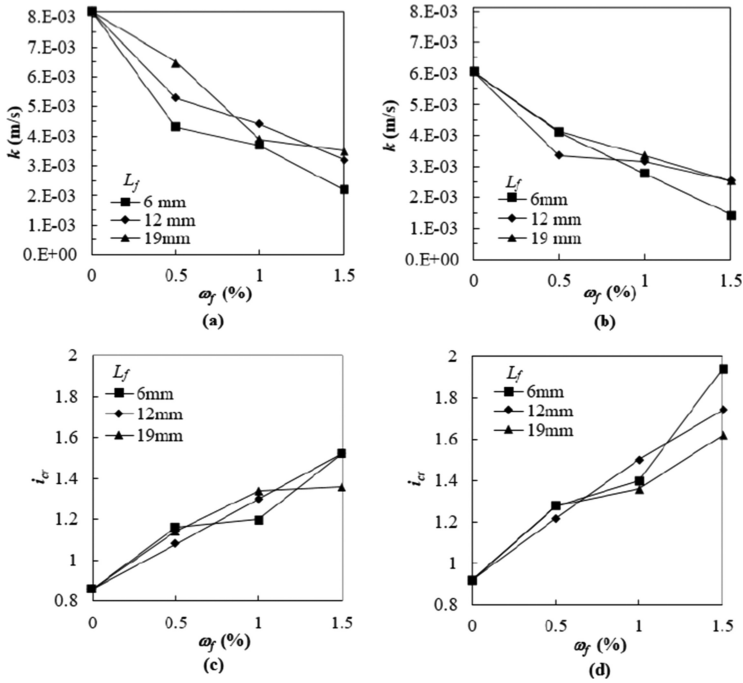
Fig. 7. Effect of fiber content on: hydraulic conductivity (a) Test Series L: (b) Test Series D, and critical hydraulic gradient (c) Test Series L, (d) Test Series D

(k ratio increases from 0.24 to 0.41) in Test Series D, respectively, as the fiber length increases from 6 to 19 mm.

Better performance in short fiber (i.e., producing a low k value) is likely because the total amount of short fiber is greater than that of long fiber at the given fiber content, resulting in short fiber possibly being able to fill more pore space than long fiber can. Finally, the variation of i_{cr} with fiber length does not show a clear trend (Figs. 8c and d), suggesting that the fiber length has only a minor influence on the i_{cr}.

In summary, test results suggest that FRS, prepared with high fiber content and short fiber length, and compacted into a dense soil state, has a superior hydraulic performance for the improvement of soil piping resistance and the reduction of seepage velocity.

3.4 Relationship Between Soil Shear Strength and Critical Hydraulic Gradient

A series of direct shear tests was performed to establish the relationship between the soil shear strength and the critical hydraulic gradient. The direct shear test was conducted in accordance with ASTM (D3080). The specimen size was 6.33 cm in diameter of and 4.66 cm in height, subjected to normal pressures of 100, 200, and 400 kPa, under a shearing rate of 1.5 mm/min. The specimens were prepared in the
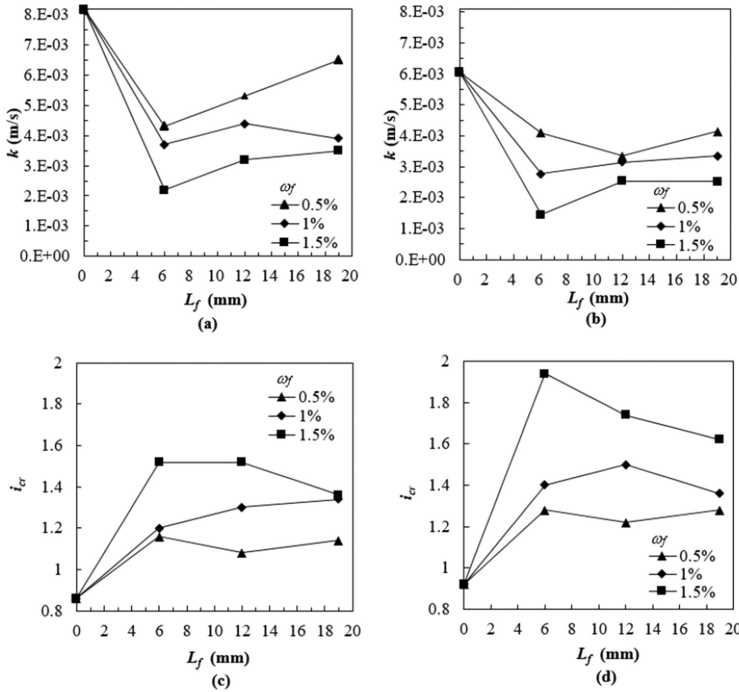
Fig. 8. Effect of fiber length on: hydraulic conductivity (a) Test Series L: (b) Test Series D, and critical hydraulic gradient (c) Test Series L, (d) Test Series D

same manner as the ones used for the seepage tests. The failure was determined corresponding to the maximum shear stress measured, or the shear stress at the relative displacement of 10 mm for the cases that no definite peak was noticed on the stress-displacement curve.

The peak soil shear strength τ_f for the specimens in the seepage test were determined from the Mohr–Coulomb failure envelopes using normal pressure in accordance with the overburden pressure at the bottom of specimens (≈ 4 kPa). After obtaining the peak shear strength of reinforced and unreinforced sand, the relationship between the soil shear strength and critical hydraulic gradient can be established (Fig. 9). As shown in Fig. 9, the i_{cr} was strongly correlated with soil τ_f. The data from specimens at different soil densities and fiber parameters fell into a unique linear relationship. This linear relationship demonstrated that the soil shear strength improvement from the fiber inclusion directly contributed to the piping resistance of FRS. This strong correlation between the soil shear strength and critical hydraulic gradient could be also related to the global and isotropic expansion failure mode of FRS. It should be noted that the established relationship cannot be extrapolated because it was established based on the results of the soil tested under low overburden pressures, representing the cases of soils at a shallow depth underneath the surface of geotechnical earth structures. Further study is required to investigate the influence of the overburden pressure on the τ_f and i_{cr} relationship.
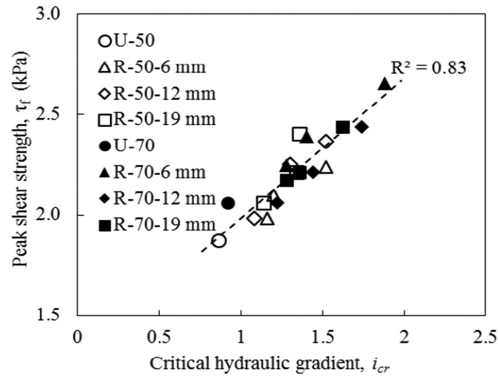
Fig. 9. Relationships between critical hydraulic gradient and soil shear strength

4 Conclusion

In this study, experimental seepage tests were conducted to investigate the hydraulic responses (i.e., piping failure mode, hydraulic conductivity, and critical hydraulic gradient) of FRS subject to seepage. Based on the test results, the following conclusions can be drawn:

(1) Unreinforced specimens had a failure mode associated with a significant soil heave and vigorous soil piping/boiling, whereas the reinforced specimens exhibited an isotropic failure mode (a uniform soil expansion) with several horizontal micro cracks developed within the specimen.

(2) Seepage test results revealed that i_{cr} increases and k decreases as the fiber content increases. The experimental results likely result from the fiber inclusion providing tensile resistance against soil piping and erosion, and restricting the seepage flow within some pore channels which were partially blocked by fibers.

(3) Test results suggested that FRS, prepared with high fiber content and short fiber length, and compacted into a dense soil state, has superior hydraulic performance in the improvement of soil piping resistance and reduction of seepage velocity.

(4) A unique linear relationship exists between i_{cr} and τ_f, indicating that soil shear strength improvement from fiber inclusion directly contributed to the piping resistance of FRS. This strong correlation between the soil shear strength and the critical hydraulic gradient is also related to the global and isotropic expansion failure mode of FRS as observed from the experimental tests.

References

ASTM D2434: Standard test method for permeability of granular soils (constant head). ASTM International, West Conshohocken

ASTM D3080: Standard test method for direct shear test of soils under consolidated drained condtions. ASTM International, West Conshohocken

ASTM D4253: Standard test methods for maximum index density and unit weight of soils using a vibratory table. ASTM International, West Conshohocken

ASTM D4254: Standard test methods for minimum index density and unit wieght of soils and calculation of relative density. ASTM International, West Conshohocken

Brandl, H.: Geosynthetics applications for the mitigation of natural disasters and for environmental protection. Geosynth. Int. **18**(6), 340–390 (2011)

Chou, J.-S., Yang, K.-H., Lin, J.-Y.: Peak shear strength of discrete fiber-reinforced soils computed by machine learning and metaensemble methods. J. Comput. Civ. Eng. **30**(6), 1–17 (2016). doi:10.1061/(ASCE)CP.1943-5487.0000595. ASCE

Consoli, N.C., Vendruscolo, M.A., Fonini, A., Rosa, F.D.: Fiber reinforcement effects on sand considering a wide cementation range. Geotext. Geomembr. **27**(3), 196–203 (2009)

Danka, J., Zhang, L.M.: Dike failure mechanisms and breaching parameters. J. Geotech. Geoenviron. Eng. **141**(9), 04015039 (2015). ASCE

Das, A., Jayashree, C., Viswanadham, B.V.S.: Effect of randomly distributed geofibers on the piping behaviour of embankments constructed with fly ash as a fill material. Geotext. Geomembr. **27**(5), 341–349 (2009)

Das, A., Viswanadham, B.V.S.: Experiments on the piping behavior of geofiber-reinforced soil. Geosynth. Int. **17**(4), 171–182 (2010)

Estabragh, A.R., Soltannajad, K., Javadi, A.A.: Improving piping resistance using randomly distributed fibers. Geotext. Geomembr. **42**(1), 15–24 (2014)

Estabragh, A.R., Soltanijad, A., Javadi, A.A.: Models for predicting the seepage velocity and seepage force in a fiber reinforced silty soil. Comput. Geotech. **75**, 174–181 (2016)

Foster, M., Fell, R., Spannagle, M.: The statistics of embankment dam failures and accidents. Can. Geotech. J. **37**(5), 1000–1024 (2000)

Furumoto, K., Miki, H., Tsuneoka, N., Obata, T.: Model test on the piping resistance of short fiber reinforced soil and its application to river levee. In: Proceeding of the 7th International Conference on Geosynthetics, Nice, France, pp. 1241–1244 (2002)

Hejazi, S.M., Sheikhzadeh, M., Abtahi, S.M., Zadhoush, A.: A simple review of soil reinforcement by using natural and synthetic fibers. Constr. Build. Mater. **30**, 100–116 (2012)

Michalowski, R., Čermák, J.: Triaxial compression of sand reinforced with fibers. J. Geotech. Geoenviron. Eng. **129**(2), 125–136 (2003). ASCE

Parekh, M., Kanning, W., Bocovich, C., Mooney, M.A., Koelewijn, A.R.: Backward erosion monitored by spatial-temporal pore pressure changes during field experiments. J. Geotech. Geoenviron. Eng. **142**(10), 1–10 (2016). doi:10.1061/(ASCE)GT.1943-5606.0001528. ASCE

Sivakumar Babu, G.L., Vasudevan, A.K.: Seepage velocity and piping resistance of coir fiber mixed soils. J. Irrig. Drain. Eng. **134**(5), 668–680 (2008). ASCE

Yetimoglu, T., Salbas, O.: A study on shear strength of sands reinforced with randomly distributed discrete fibers. Geotext. Geomembr. **21**(2), 103–110 (2003)

Zornberg, J.: Discrete framework for limit equilibrium analysis of fiber-reinforced soil. Géotechnique **52**(8), 593–604 (2002)